



Coarse-grained molecular simulation of the effect of liquid crystal molecular pitch on structure in cylindrical confinement

Takumi Sato ^{*}, Hiroaki Tsujinoue, and Noriyoshi Arai [†]

Department of Mechanical Engineering, Keio University, Yokohama, Kanagawa 223-8522, Japan

Kazuaki Z. Takahashi 

Research Center for Computational Design of Advanced Functional Materials, National Institute of Advanced Industrial Science and Technology (AIST), Tsukuba, Ibaraki 305-8568, Japan



(Received 29 March 2024; accepted 14 June 2024; published 8 July 2024)

Blue phases (BPs) consist of three-dimensional self-assembled structures formed by a double-twisted columnar arrangement of liquid crystal molecules. Although their unique optical and structural properties render BPs particularly useful for applications such as liquid crystal displays, BPs typically appear in a narrow temperature range between the isotropic and nematic phases. This thermodynamic instability impedes their practical applicability. However, the simulations we present here showed that, in a quasi-one-dimensional system confined to nanospace, a phase equivalent to the BP appears and persists between the nematic and smectic phases. Confinement to a nanotube (NT) with a relatively small radius enables the BP to be maintained over a wide temperature range, whereas for an NT with a relatively larger radius, the BP appears only in a very narrow temperature range between the aforementioned phases. We additionally showed that the pitch of the BP is dependent on and can be controlled by adjusting the radius of the NTs. This finding has significant implications for the potential application of these materials in fields such as photonics and chiral separation technologies.

DOI: [10.1103/PhysRevE.110.014701](https://doi.org/10.1103/PhysRevE.110.014701)

I. INTRODUCTION

The blue phase (BP), one of the phases exhibited by molecules with liquid-crystalline properties, is an intriguing and complex area in condensed matter physics that offers a unique blend of physical peculiarities and promising engineering applications [1–4]. Liquid crystals (LCs), characterized by their ability to exhibit distinct phases with intriguing optical and structural properties, have become the subject of extensive research and technological exploration. Among these phases, the BP is unique owing to its three-dimensional complexity, which comprises a network of multitwisted cylinders and discretization lines of LC molecules.

Situated in the narrow temperature range between the isotropic and chiral nematic or cholesteric phases, the BP exhibits a fascinating range of physical properties. The three known thermodynamically stable variants thereof, BPI, BPII, and BPIII, each have a unique structural architecture [5]. Specifically, BPI and BPII have a three-dimensional periodic structure characterized by simple cubic and body-centered cubic symmetry, whereas BPIII adopts an amorphous state with a local cubic lattice structure [6–8]. In particular, the BP has an optically isotropic structure with a response time ten times faster than that of the conventional nematic phase, a feature that has attracted considerable interest from researchers.

However, BPs have found limited application to date because they typically occur in a narrow temperature range

of approximately 1 °C between the cholesteric phase and isotropic liquid. This narrow temperature range, and the associated instability of the phase, limits its practical applicability. However, Kikuchi *et al.* [9] reported a polymer-stabilized BP of which the temperature range was extended to approximately 60 °C by polymerizing the LC molecule in the BP. In addition, Coles *et al.* [10] reported a compound with a dimeric structure, which effectively involved two biphenyl moieties, and which exhibited a BP with a temperature range of 40 °C. Blue phases are compelling candidates for advanced photonic materials because of their optical isotropy, combined with their fast response time. In this regard, the work of Wang *et al.* [11], who reported the fabrication of polymer-stabilized BPI films with self-assembled 3D nanostructures and the achievement of an electrically tunable photonic band gap, represents a crucial step toward practical engineering applications. In recent years, microsensors and color actuators using BPs have been actively investigated [12,13]. Orzechowski *et al.* [14] demonstrated that the addition of gold nanoparticles (NPs) as a dopant to LCs with a BP has the effect of elongating the BP lattice and increasing the wavelength of light reflection. They additionally found that the use of NPs as dopants significantly increased the thermal stability of the phase. These properties highlight the important role BPs could play in the development of next-generation displays and photonics technologies.

Fluids confined to nanoscale spaces are widely recognized to be capable of exhibiting new phases that are not observed in bulk systems [15,16]. This phenomenon extends to general fluids, such as water, in which abnormal behavior occurs owing to the nanoconfinement effect [17–19]. Confinement within a nanotube of an LC molecule representing a functional

^{*}Contact author: sato8322@keio.jp

[†]Contact author: arai@mech.keio.ac.jp

material is expected to allow much richer morphologies to emerge. This is because the dimensional constraint imposed by the nanotube influences not only the thermodynamic equilibrium but also the additional self-assembling nature of the LC molecules [20–24].

For example, Fukuda and Žumer [21] theoretically demonstrated that highly chiral LCs can host stable quasi-two-dimensional (Q2D) skyrmion lattices in a two-dimensional confined nanoslit system. Their investigation covered a range of temperatures and thicknesses in a confinement system using numerical calculations. They concluded that regular Q2D skyrmion lattices with hexagonal or rectangular symmetries are thermodynamically stable. Salgado-Blanco *et al.* [24] performed Monte Carlo simulations of a spherical droplet formed by a discotic liquid crystal (DLC). Their results showed that lowering the temperature induced orientationally ordered liquid layers, which led to the formation of nematic spherical shells. As the temperature decreased, they observed a first-order isotropic-nematic transition in the central region of the droplet, followed by a nematic-columnar transition. Both transitions occurred at lower temperatures than in an infinite DLC system.

In addition to the aforementioned discoveries, several research groups recently reported the confinement of cholesteric liquid crystal (CLC) molecules, which are LC molecules with intramolecular twists, to nanospaces [25–28]. In particular, Tsujinoue *et al.* [25] carried out coarse-grained molecular simulations on a quasi-one-dimensional (Q1D) nanotube system, and observed the variations in the morphological behavior of CLCs as a function of the temperature and nanotube radius. Their study revealed a novel self-assembled structure with cylindrical (or ringlike) defects instead of lines, thereby providing insights into intensity control in Q1D systems. Palacio-Betancur *et al.* [27] theoretically studied chiral LCs confined to cylindrical and toroidal cavities, and discovered new morphologies resulting from the interplay between the confinement curvature and twisted material. Their study enabled them to categorize these morphologies according to three ratios, and provided insights into their properties to enable them to explore the potential of forming chiral ribbons, particularly helical ribbons, for directed assembly.

However, the pitch of an LC with a BP significantly influences its electro-optical properties, which play a crucial role in sensing and photonics applications. An analysis based on a molecular-level model of the pitch formed by CLCs has not yet been reported. In this study, we constructed a Q1D system by confining the CLC molecular models to nanotubes based on our previous work [25]. We observed the variation in the morphology and pitch formed by the CLC molecules inside the nanotubes with the temperature and radius of the nanotubes. Conditions for pitch control in confined systems and the emergence of double-twisted structures with properties similar to the blue phase are discussed.

II. METHOD AND MODELS

A. Coarse-grained molecular simulation

In this study, we used the dissipative particle dynamics (DPD) method [29–31], a coarse-grained molecular

simulation technique, to reproduce the diverse phase behaviors of cholesteric liquid crystal (CLC) molecules. Numerical methods are powerful mesoscopic simulation tools for reproducing fluid events over a wide range of spatiotemporal scales by tracking the motion of coarse-grained particles (composed of a group of atoms or molecules). Various studies have investigated the morphological behavior of LCs at the mesoscopic level, such as the phase separation of rod-coil polymers [32–35], interaction between surfactants and LCs [22,23,35–37], and self-assembly upon confinement to a nanospace [25,38–40] using the DPD method. The fundamental equation that forms the basis of the DPD method is identical to Newton's equation of motion. Each DPD bead (corresponding to a coarse-grained particle) is subjected to conservative (\mathbf{F}_{ij}^C), dissipative (\mathbf{F}_{ij}^D), and random forces (\mathbf{F}_{ij}^R). Newton's equation of motion for particle i is given by

$$m_i \frac{d\mathbf{v}_i}{dt} = \mathbf{f}_i = \sum_{j \neq i} (\mathbf{F}_{ij}^C + \mathbf{F}_{ij}^D + \mathbf{F}_{ij}^R) + \mathbf{F}_i^E. \quad (1)$$

In Eq. (1), m is the mass, \mathbf{v} is the velocity, \mathbf{F}^C is the conservative force, \mathbf{F}^D is the dissipative force, \mathbf{F}^R is the random force, and \mathbf{F}^E is the external force used to simulate the nanotube system. The force acting on the CLC molecule is the sum of all the inter-coarse-grained particle forces between particles i and j . The conservative force (\mathbf{F}_{ij}^C) is

$$\mathbf{F}_{ij}^C = \begin{cases} -a_{ij} \left(1 - \frac{|\mathbf{r}_{ij}|}{r_c}\right) \mathbf{n}_{ij}, & |\mathbf{r}_{ij}| \leq r_c \\ 0, & |\mathbf{r}_{ij}| > r_c, \end{cases} \quad (2)$$

where a_{ij} is a parameter to determine the magnitude of the repulsive force between particles i and j , r_c is the cut-off distance, and $\mathbf{r}_{ij} = \mathbf{r}_j - \mathbf{r}_i$ and $\mathbf{n}_{ij} = \mathbf{r}_{ij}/|\mathbf{r}_{ij}|$. In this study, the interaction parameter between each particle (a_{ij}) is $a_{ij} = 25k_B T/r_c$ and the interaction parameter between the wall and the particles ($a_{\text{wall},p}$) is $a_{\text{wall},p} = 100k_B T/r_c$. The dissipative force (\mathbf{F}_{ij}^D) and random force (\mathbf{F}_{ij}^R) are given as follows:

$$\mathbf{F}_{ij}^D = \begin{cases} -\gamma \omega^D(|\mathbf{r}_{ij}|) (\mathbf{n}_{ij} \cdot \mathbf{v}_{ij}) \mathbf{n}_{ij}, & |\mathbf{r}_{ij}| \leq r_c \\ 0, & |\mathbf{r}_{ij}| > r_c \end{cases} \quad (3)$$

and

$$\mathbf{F}_{ij}^R = \begin{cases} \sigma \omega^R(|\mathbf{r}_{ij}|) \zeta_{ij} \Delta t^{-1/2} \mathbf{n}_{ij}, & |\mathbf{r}_{ij}| \leq r_c \\ 0, & |\mathbf{r}_{ij}| > r_c. \end{cases} \quad (4)$$

In Eqs. (3) and (4), $\mathbf{v}_{ij} = \mathbf{v}_j - \mathbf{v}_i$, γ is the friction coefficient, σ is the noise amplitude, ζ_{ij} is a random number based on the Gaussian distribution, and Δt is the time step.

Here, ω^D and ω^R are the distance-dependent weight functions for \mathbf{F}_{ij}^D and \mathbf{F}_{ij}^R , given by

$$\omega^D(r) = [\omega^R(r)]^2 = \begin{cases} \left[1 - \frac{|\mathbf{r}_{ij}|}{r_c}\right]^2, & |\mathbf{r}_{ij}| \leq r_c \\ 0, & |\mathbf{r}_{ij}| > r_c. \end{cases} \quad (5)$$

The temperature is controlled by the coupling of dissipative and random forces. The friction parameter γ and noise parameter σ are related to the fluctuation-dissipation theorem:

$$\sigma^2 = 2\gamma k_B T, \quad (6)$$

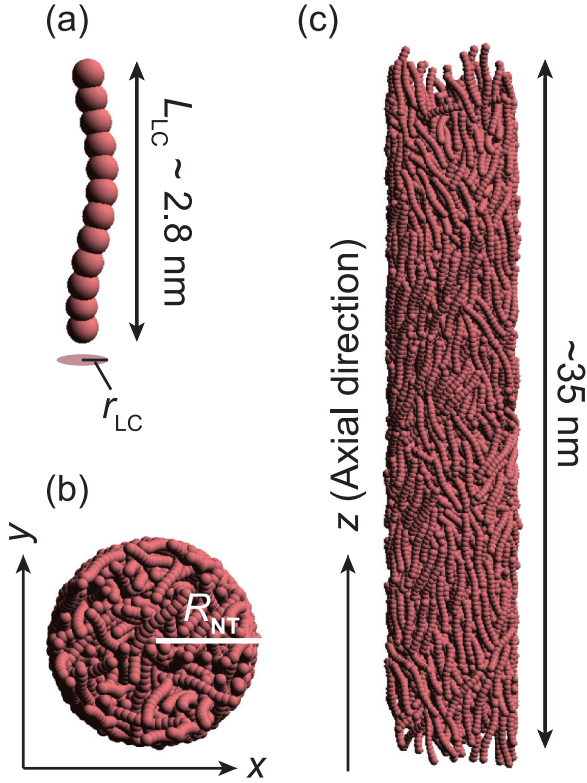


FIG. 1. Cholesteric liquid crystal (CLC) model and system: (a) CLC molecular model composed of twelve particles; the radius of the helix r_{LC} is constant ($r_{LC} \sim 0.1$ nm). (b) Top view and (c) side view of quasi-one-dimensional system.

where $k_B T$ is Boltzmann's constant and T is the temperature.

We applied an external force (\mathbf{F}_i^E) to realize Q1D nanotube systems. Hence, the inner wall of the cylindrical nanotube was considered to be smooth. The potential function of the smooth wall was derived based on that of a structured wall by summing the DPD forces between the respective particles and the wall particles [41,42]. Integration of this summed force yielded the force between the DPD particle and the smooth wall (within the cut-off distance r_c), that is, $\mathbf{F}_i^E = \frac{1}{6}\pi\rho_{\text{wall}}\alpha_{\text{wall,p}}(-R^4 + 2R^3 - 2R + 1)\mathbf{R}/R$ where ρ_{wall} is the number density of the structured wall, $\alpha_{\text{wall,p}}$ is the interaction parameter between the wall and the DPD particle, \mathbf{R} is the normal vector from the particle to the wall surface, and $R = |\mathbf{R}|$ is the distance between the wall and the particle.

In general, reduced units are used to report the DPD results. The DPD unit of length is the cut-off radius (or particle diameter) r_c , the unit of mass is the particle mass m , and $k_B T$. Thus, the unit of time (τ) is defined as $\sqrt{mr_c^2/k_B T}$. Because we used the same CLC model as in our previous work, we scaled the length and temperature from reduced to physical units in the same manner as in [25,43].

B. Simulation model

Referring to our previous work [25], the helix in the CLC model used in this simulation has the radius $r_{LC} \sim 0.09$ nm and length $L_{LC} \sim 2.8$ nm (the number of pitches is 1.0), as shown in Fig. 1(a). A single CLC model was composed of 12

TABLE I. Number of particles used for each system. Here, R_{NT} is the radius of the nanotube in nm and N is total number of beads.

R_{NT}	N	R_{NT}	N
2.85	7536	5.16	24 768
3.02	8508	5.33	26 508
3.20	9540	5.51	28 308
3.38	10 632	5.69	30 156
3.56	11 784	6.05	34 044
3.73	12 984	6.40	38 172
3.91	14 256	6.76	42 528
4.09	15 576	7.11	47 124
4.27	16 968	7.47	51 960
4.45	18 408	7.82	57 024
4.62	19 908	8.18	62 316
4.80	21 468	8.54	67 860
4.98	23 088	8.89	73 632

DPD particles because a twisted rigid model is often used to simulate chiral liquid crystals [44,45]. In addition, each LC was treated as a rigid body in the simulations. Stable CLC phases were observed in the CLC model for these parameters under a range of appropriate thermodynamic conditions [25].

In the DPD simulation of a quasi-one-dimensional (Q1D) nanotube system, periodic boundary conditions were applied in the axial direction (z) to reproduce nanotubes of infinite lengths. In this study, the phase behavior of CLC molecules was investigated for 16 different nanotube radii, R_{NT} , ranging from 2.58 to 5.01 nm. The numbers of particles used in our simulation are listed in Table I. The initial configuration was random, as shown in Figs. 1(b) and 1(c). To obtain random structures, each system was initialized at 98.5 °C for $t \simeq 352$ ns.

The system density ρ was maintained constant for each value of R_{NT} . To prevent the LC molecules from penetrating the NT wall, ρ_{wall} was chosen to be 10.0 [42,46], which is more than three times larger than the inner value. We set Δt , γ , σ to 0.04, 4.5, and 3.0, respectively.

All the simulations were performed in a constant-volume and constant-temperature ensemble. We simulated the cooling of the Q1D system from 98.5 °C to 55.5 °C. The total number of steps for one R_{NT} was calculated to be 6×10^6 steps, or 352 ns for each temperature. The cooling rate, which was selected based on a previous study [47], is known to be higher in molecular simulations than that in typical experiments. We performed several simulations with different initial configurations to ensure true equilibration. Starting from different configurations agreed well with the formation of self-assembled structures.

III. RESULTS AND DISCUSSION

A. Phase diagram of cholesteric liquid crystals confined to a nanotube

We first investigated the phase behavior of a CLC in nanospace to determine whether a BP would form and the conditions under which it would emerge. Figure 2 shows the quantitative phase diagram of the system in which the CLCs are confined to NTs. The temporal variation in the potential

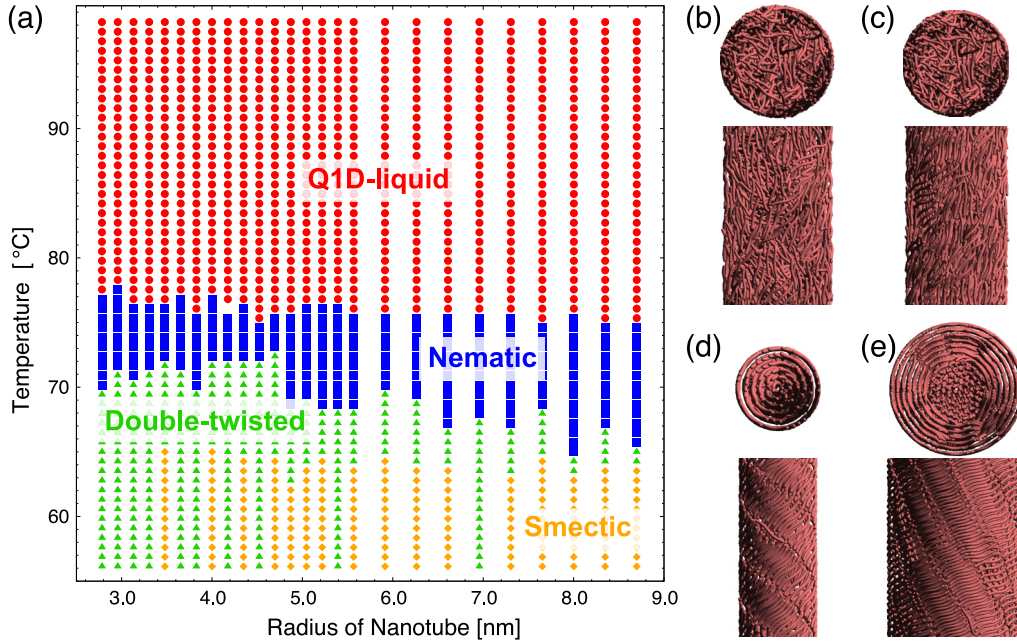


FIG. 2. (a) Phase diagram of CLC confined to a nanotube (NT): radius of NT versus temperature. The red circles, blue squares, green triangles, and orange diamonds represent Q1D-liquid (b), nematic (c), double-twisted (d), and smectic (e) phases, respectively.

energy was used to determine the stable state of each phase. In this study, we employ the orientational order parameter as a method for layer classification, as has been done in previous studies [25].

During the cooling process, three phase transitions were observed: from the Q1D liquid phase to the nematic phase, from the nematic phase to the double-twisted phase, and from the double-twisted phase to the smectic phase. The phase transition temperatures depend on the confinement radius R_{NT} .

Regardless of the value of R_{NT} , the Q1D liquid phase, in which the liquid crystal molecules were randomly oriented, emerged at high temperatures ($T \geq 78$ °C). As cooling progressed, the LC molecules in the nanotube gradually became increasingly oriented. When T is ~ 76 °C, the CLC systems transition to the nematic phase (as shown in Fig. 2), in which the long axis of the LC molecules is oriented in a certain direction but the center of gravity of the LC molecules is not regular. Upon cooling, the onset of the nematic phase for most R_{NT} values starts at T of approximately 77 °C. The temperature range of the nematic phase increased with increasing R_{NT} .

Further cooling was characterized by the formation of twisted structures of LC molecules near the wall surface, with the eventual formation of double-twisted structures (Fig. 2). The double-twisted structure is the basic structure of the BP formed by doubly twisted LC molecules. This double-twisted structure was formed for all values of R_{NT} s. For some values of R_{NT} , the LC molecules exhibited two different structural orientations: in the first, the molecules were oriented obliquely to the long axis of the NT, whereas in the other, the molecules were aligned with the long axis of the NT to form a smectic phase (Fig. 2). These two orientations were not interchangeable, even at lower temperatures, with no transition from double-twisted structure to smectic phase. In general, in a spatially unconstrained LC phases, LC molecules are oriented in the same direction at low temperatures. However,

in a confined state, there are two types of LC molecules: those that are affected by the wall surface and those that are not. Especially for confinement on a curved surface such as NT, LC is oriented at a certain inclination, not in the same direction as NT, depending on the pitch and its torsional radius. Therefore, two different orientations appear at low temperatures, forming a nematic layer. But when NT is sufficiently small, all LC molecules are affected by the wall surface, and a double-twisted structure is formed. In other words, for systems confined to small NT, a double-twisted structure with the same characteristics as those of the blue phase can be achieved over a wide temperature range.

B. Angle distribution in the radial direction

To clarify the difference between the nematic and double-twisted phases, the orientation of LC molecules from the center to the wall of the NT was calculated. The distribution of the angle θ between the LC molecules and long axis of the NT in the radial direction is plotted in Fig. 3. Here, $r = 0$ corresponds to the center of the NT. Figures 3(a) and 3(b) show the angular distributions of the confinement radius at which the double-twisted structure is formed at low T ($R_{NT} \simeq 4.17$ nm) and the confinement radius at which the smectic phase is formed at low T ($R_{NT} \simeq 5.21$ nm).

For both of these values of R_{NT} , in the high-temperature Q1D liquid phase, θ in the central region was approximately 60° and decreased gently toward the wall surface, whereas near the wall, the value of θ was approximately 30°. This implies that, near the wall, the LC molecules were approximately aligned with the long axis of the NT, whereas in the central region, the tilt angle with respect to the long axis of the NT was larger. As cooling proceeded, the LC molecules at the center of the NT became increasingly aligned. At approximately 76.6 °C, the Q1D liquid phase underwent the transition

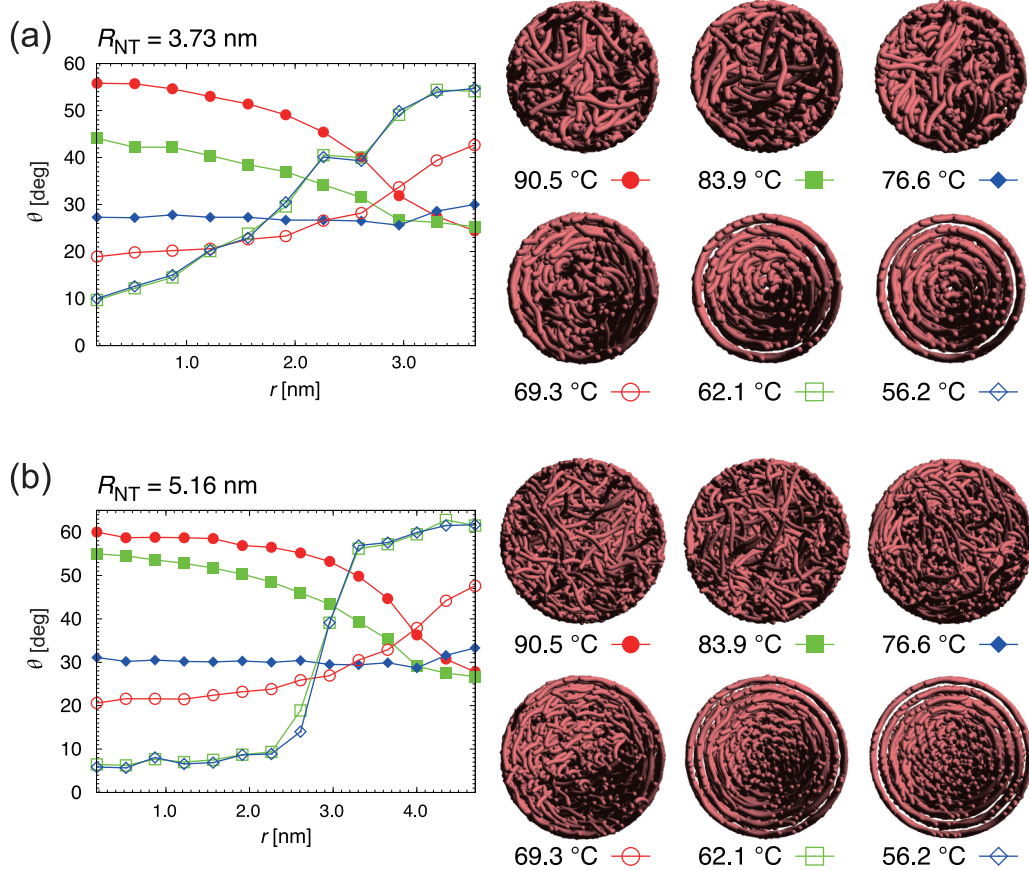


FIG. 3. Angle θ between orientation of the LC molecules and the axial direction for (a) $R_{NT} = 3.73$ nm and (b) $R_{NT} = 5.16$ nm. On the right: snapshots of the top view for each temperature.

to the nematic phase in which θ remained almost constant ($\theta \sim 30^\circ$) throughout the interior of the NT.

At even lower temperatures ($T < 70^\circ\text{C}$), different behaviors were observed for $R_{NT} = 4.17$ and 5.21 nm. At $R_{NT} = 4.17$ nm [Fig. 3(a)], as the system cools, the double-twisted structure is formed, with a constant r - θ gradient. Below $T = 62^\circ\text{C}$, the gradient is constant with values of $\theta = 10^\circ$ at the center and $\theta = 55^\circ$ at the walls. On the other hand, for $R_{NT} = 5.21$ nm, as cooling progressed, the LC molecules oriented in the axial direction occupied a larger area in the central region of the NT ($r < 2.5$ nm). This corresponded to the smectic phase.

C. Pitch of the spiral structure

Figure 4 shows the relationship between the helical pitch (p) formed by CLCs in the NT and R_{NT} . As R_{NT} increased, p gradually decreased and became almost constant ($p \sim 3$) when R_{NT} exceeded approximately 6.0 . This suggests that the spiral pitch formed by CLCs can be controlled by adjusting the spatial constraint.

IV. CONCLUSION

In this study, we used dissipative particle dynamics to investigate the behavior of a film of liquid crystal (LC) molecules in a quasi-one-dimensional (Q1D) system. The

simulation showed that confinement of the LC molecules in a Q1D system can lead to the formation of a double-twisted structure, with characteristics that resemble those of the blue phase, over a broad temperature range. Although the temperature range in which this structure prevailed varied depending on the confinement radius (R_{NT}), the double-twisted structure formed and existed in a temperature range of more than 10°C ($T \geq 60 \sim 70$) when $R_{NT} = 3.73$ nm. The spiral pitch of the cholesteric LC can be controlled by R_{NT} , which

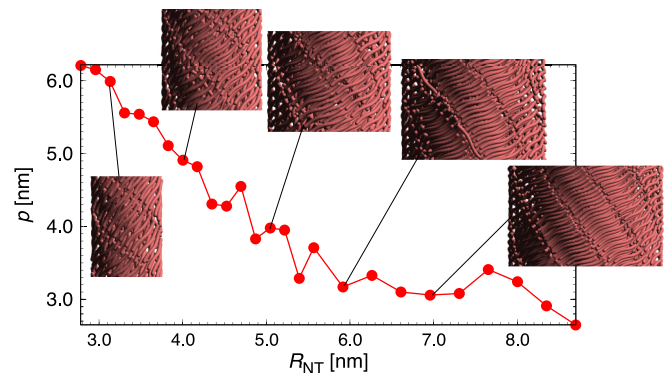


FIG. 4. Relationship between the pitch (p) of the helix formed in NT and radius of NT (R_{NT}). Insets: snapshots of a number of representative side views.

decreases as R_{NT} increases and stabilizes at $p = 3.0$ nm. This result opens up the possibility of creating nanodevices in which the wavelength of the light transmitted in the nanotubes can be precisely controlled within the visible light

spectrum by appropriately selecting the degree of confinement. Our findings have significant implications for the potential application of these materials in sensors and photonics technologies.

-
- [1] D. C. Wright and N. D. Mermin, Crystalline liquids: the blue phases, *Rev. Mod. Phys.* **61**, 385 (1989).
- [2] A. J. Berresheim, M. Müller, and K. Müllen, Polyphenylene nanostructures, *Chem. Rev.* **99**, 1747 (1999).
- [3] H. K. Bisoyi and Q. Li, Liquid crystals: Versatile self-organized smart soft materials, *Chem. Rev.* **122**, 4887 (2022).
- [4] K. Bagchi, T. Emeršič, J. A. Martínez-González, J. J. de Pablo, and P. F. Nealey, Functional soft materials from blue phase liquid crystals, *Sci. Adv.* **9**, eadh9393 (2023).
- [5] P. P. Crooker, Chirality in Liquid Crystals. Partially Ordered Systems, in *Blue Phases*, edited by H. S. Kitzerov and C. Bahr (Springer-Verlag, New York, NY, 2001), pp. 186–222.
- [6] E. Dubois-violette and B. Pansu, Frustration and related topology of blue phases, *Molecular Crystals and Liquid Crystals Incorporating Nonlinear Optics* **165**, 151 (1988).
- [7] H.-S. Kitzerow, P. P. Crooker, and G. Heppke, Line shapes of field-induced blue-phase-III selective reflections, *Phys. Rev. Lett.* **67**, 2151 (1991).
- [8] R. M. Hornreich, Surface interactions and applied-field effects in cholesteric helicoidal and blue phases, *Phys. Rev. Lett.* **67**, 2155 (1991).
- [9] H. Kikuchi, M. Yokota, Y. Hisakado, H. Yang, and T. Kajiyama, Polymer-stabilized liquid crystal blue phases, *Nat. Mater.* **1**, 64 (2002).
- [10] H. Coles and M. Pivnenko, Liquid crystal ‘blue phases’ with a wide temperature range, *Nature (London)* **436**, 997 (2005).
- [11] M. Wang, C. Zou, J. Sun, L. Zhang, L. Wang, J. Xiao, F. Li, P. Song, and H. Yang, Asymmetric tunable photonic bandgaps in self-organized 3D nanostructure of polymer-stabilized blue phase I modulated by voltage polarity, *Adv. Funct. Mater.* **27**, 1702261 (2017).
- [12] L. L. Ma, C. Y. Li, J. T. Pan, Y. E. Ji, C. Jiang, R. Zheng, Z. Y. Wang, Y. Wang, B. X. Li, and Y. Q. Lu, Self-assembled liquid crystal architectures for soft matter photonics, *Light Sci. Appl.* **11**, 270 (2022).
- [13] P. Zhang, L. T. de Haan, M. G. Debije, and A. P. Schenning, Liquid crystal-based structural color actuators, *Light Sci. Appl.* **11**, 248 (2022).
- [14] K. Orzechowski, M. Tupikowska, O. Strzeżysz, T. M. Feng, W. Y. Chen, L. Y. Wu, C. T. Wang, E. Otón, M. M. Wójcik, M. Bagiński, P. Lesiak, W. Lewandowski, and T. R. Woliński, Achiral nanoparticle-enhanced chiral twist and thermal stability of blue phase liquid crystals, *ACS Nano* **16**, 20577 (2022).
- [15] M. W. Maddox and K. E. Gubbins, A molecular simulation study of freezing/melting phenomena for Lennard-Jones methane in cylindrical nanoscale pores, *J. Chem. Phys.* **107**, 9659 (1997).
- [16] R. J. Mashl, S. Joseph, N. R. Aluru, and E. Jakobsson, Anomalous immobilized water: A new water phase induced by confinement in nanotubes, *Nano Lett.* **3**, 589 (2003).
- [17] K. Koga, G. T. Gao, H. Tanaka, and X. C. Zeng, Formation of ordered ice nanotubes inside carbon nanotubes, *Nature (London)* **412**, 802 (2001).
- [18] K. Mochizuki and K. Koga, Solid-liquid critical behavior of water in nanopores, *Proc. Natl. Acad. Sci. USA* **112**, 8221 (2015).
- [19] K. Nomura, T. Kaneko, J. Bai, J. S. Francisco, K. Yasuoka, and X. C. Zeng, Evidence of low-density and high-density liquid phases and isochore end point for water confined to carbon nanotube, *Proc. Natl. Acad. Sci. USA* **114**, 4066 (2017).
- [20] S. Kralj and S. Žumer, The stability diagram of a nematic liquid crystal confined to a cylindrical cavity, *Liq. Cryst.* **15**, 521 (1993).
- [21] J. ichi Fukuda and S. Žumer, Quasi-two-dimensional skyrmion lattices in a chiral nematic liquid crystal, *Nat. Commun.* **2**, 246 (2011).
- [22] T. Inokuchi and N. Arai, Liquid-crystal ordering mediated by self-assembly of surfactant solution confined in nanodroplet: a dissipative particle dynamics study, *Mol. Simul.* **43**, 1218 (2017).
- [23] H. Tsujinoue, T. Inokuchi, and N. Arai, Polymorphic transitions mediated by surfactants in liquid crystal nanodroplet, *Liq. Cryst.* **46**, 1428 (2019).
- [24] D. Salgado-Blanco, E. Díaz-Herrera, J. A. Martínez-González, and C. I. Mendoza, Phase transitions and topological defects in discotic liquid crystal droplets with planar anchoring: a Monte Carlo simulation study, *Soft Matter* **19**, 5916 (2023).
- [25] H. Tsujinoue, T. Nozawa, and N. Arai, Cylindrical defect structures formed by chiral nematic liquid crystal in quasi-one-dimensional nanotubes, *Phys. Chem. Chem. Phys.* **22**, 16896 (2020).
- [26] P. E. Brumby, A. Kowaguchi, T. Nozawa, K. Yasuoka, and H. H. Wensink, Pre-smectic ordering and the unwinding helix in Monte Carlo simulations of cholesteric liquid-crystals, *J. Phys. Chem. B* **127**, 7194 (2023).
- [27] V. Palacio-Betancur, J. C. Armas-Pérez, J. P. Hernández-Ortiz, and J. J. de Pablo, Curvature and confinement effects on chiral liquid crystal morphologies, *Soft Matter* **19**, 6066 (2023).
- [28] H. B. Kolli, E. Frezza, G. Cinacchi, A. Ferrarini, A. Giacometti, and T. S. Hudson, Communication: From rods to helices: Evidence of a screw-like nematic phase, *J. Chem. Phys.* **140**, 081101 (2014).
- [29] P. J. Hoogerbrugge and J. M. V. A. Koelman, Simulating microscopic hydrodynamic phenomena with dissipative particle dynamics, *Europhys. Lett.* **19**, 155 (1992).
- [30] P. Español and P. Warren, Statistical mechanics of dissipative particle dynamics, *Europhys. Lett.* **30**, 191 (1995).
- [31] R. D. Groot and P. B. Warren, Dissipative particle dynamics: Bridging the gap between atomistic and mesoscopic simulation, *J. Chem. Phys.* **107**, 4423 (1997).
- [32] Q. Zhang, J. Lin, L. Wang, and Z. Xu, Theoretical modeling and simulations of self-assembly of copolymers in solution, *Prog. Polym. Sci.* **75**, 1 (2017).
- [33] P. Xu, J. Lin, L. Wang, and L. Zhang, Shear flow behaviors of rod-coil diblock copolymers in solution: A nonequilibrium

- dissipative particle dynamics simulation, *J. Chem. Phys.* **146**, 184903 (2017).
- [34] L. Wang, Z. Tang, D. Li, J. Lin, and Z. Guan, Adsorption and ordering of amphiphilic rod-coil block copolymers on a substrate: Conditions for well-aligned stripe nanopatterns, *Nanoscale* **12**, 13119 (2020).
- [35] J. Zhang, S. Li, Y. Yin, L. Xiang, F. Xu, and Y. Mai, One-dimensional helical nanostructures from the hierarchical self-assembly of an achiral “rod-coil” alternating copolymer, *Macromol. Rapid Commun.* **43**, 2200437 (2022).
- [36] Z. Sumer and A. Striolo, Manipulating molecular order in nematic liquid crystal capillary bridges: Via surfactant adsorption: Guiding principles from dissipative particle dynamics simulations, *Phys. Chem. Chem. Phys.* **20**, 30514 (2018).
- [37] R. L. Anderson, D. S. Gunn, T. Taddese, E. Lavagnini, P. B. Warren, and D. J. Bray, Phase behavior of alkyl ethoxylate surfactants in a dissipative particle dynamics model, *J. Phys. Chem. B* **127**, 1674 (2023).
- [38] Z. Zhang, H. Guo, and E. Nies, Mesoscopic simulations of temperature-dependent anchoring and wetting behavior at aqueous-liquid crystal interfaces in the presence of a rod-coil amphiphilic monolayer, *RSC Advances* **8**, 42060 (2018).
- [39] C. Nam, W. B. Lee, and Y. J. Kim, Self-assembly of rod-coil diblock copolymer-nanoparticle composites in thin films: dissipative particle dynamics, *Soft Matter* **17**, 2384 (2021).
- [40] S. Chen, J. Zhang, H. Liu, T. Qiu, H. Tang, and Z. Zhang, Dissipative particle dynamics simulation of the sensitive anchoring behavior of smectic liquid crystals at aqueous phase, *Molecules* **27**, 7433 (2022).
- [41] N. Arai, K. Yasuoka, and X. C. Zeng, Self-assembly of surfactants and polymorphic transition in nanotubes, *J. Am. Chem. Soc.* **130**, 7916 (2008).
- [42] N. Arai, K. Yasuoka, and X. C. Zeng, Self-assembly of triblock Janus nanoparticle in nanotube, *J. Chem. Theory Comput.* **9**, 179 (2013).
- [43] R. Groot and K. Rabone, Mesoscopic simulation of cell membrane damage, morphology change and rupture by nonionic surfactants, *Biophys. J.* **81**, 725 (2001).
- [44] S. Dussi and M. Dijkstra, Entropy-driven formation of chiral nematic phases by computer simulations, *Nat. Commun.* **7**, 11175 (2016).
- [45] H. B. Kolli, G. Cinacchi, A. Ferrarini, and A. Giacometti, Chiral self-assembly of helical particles, *Faraday Discuss.* **186**, 171 (2016).
- [46] Y. Kobayashi and N. Arai, Self-assembly of Janus nanoparticles with a hydrophobic hemisphere in nanotubes, *Soft Matter* **12**, 378 (2016).
- [47] C. Soto-Figueroa, M. del Rosario Rodríguez-Hidalgo, J.-M. Martínez-Magadán, and L. Vicente, Dissipative particle dynamics study of order-order phase transition of BCC, HPC, OBDD, and LAM structures of the poly(styrene)-poly(isoprene) diblock copolymer, *Macromolecules* **41**, 3297 (2008).